Available online at www.sciencedirect.com
ScienceDirect
Journal of Computational Physics 225 (2007) 1736–1752
JOURNAL OF COMPUTATIONAL PHYSICS
www.elsevier.com/locate/jcp

A method for obtaining three-dimensional computational equilibrium of non-neutral plasmas using WARP

K. Gomberoff [a,*], J. Wurtele [a], A. Friedman [b], D.P. Grote [b], J.-L. Vay [c]

[a] *Center for Beam Physics, Lawrence Berkeley National Laboratory and Department of Physics, UC Berkeley, Berkeley, CA 94720, United States*
[b] *Fusion Energy Program, Lawrence Livermore National Laboratory, Livermore, CA 94550, United States*
[c] *Lawrence Berkeley National Laboratory, Berkeley, CA 94720, United States*

Received 15 September 2006; received in revised form 18 January 2007; accepted 19 February 2007
Available online 14 March 2007

Abstract

Computer simulation studies of the stability and transport properties of trapped non-neutral plasmas require the numerical realization of a three-dimensional plasma distribution. This paper presents a new numerical method for obtaining, without an explicit model for physical collisions in the code, a low noise three-dimensional computational equilibrium distribution. This requires both the loading of particles into an idealized distribution and the relaxation from that distribution toward an approximate numerical equilibrium. The equilibrium can then be modified through a slow change of system parameters, to generate other equilibria. In the present, work we apply this method to a UC Berkeley experiment on electron confinement in magnetic geometries appropriate for the ALPHA anti-hydrogen experiment, using the three-dimensional particle-in-cell code WARP. WARP's guiding center mover and its option to switch between different solvers during a simulation are highly valuable because they speed up the simulations; they enable the practical use of the new technique for generating numerical equilibrium states of trapped non-neutral plasmas.

Keywords: WARP; PIC code; Particle-in-cell; Equilibrium; Numerical equilibrium; Non-neutral plasmas; Plasma trap; Numerical collisions; Three dimensional; Non-uniform field

1. Introduction

The equilibrium of a non-neutral plasma in a Penning–Malmberg trap has been the subject of a number of studies (see for example [1–4]). Additional confining elements in such traps, such as mirror coils or magnetic multipole fields, can affect the equilibrium and the transport properties of the plasma. For example, a mirror field which has been extensively studied in the fusion community has been suggested to cause transport in such traps [1]. The equilibrium properties of the non-neutral plasma in a trap with a mirror have been studied

* Corresponding author. Current address: Physics Department, Technion, 32000 Haifa, Israel. Tel.: +1 972 4 8743101.
E-mail address: katia@physics.technion.ac.il (K. Gomberoff).

0021-9991/$ - see front matter © 2007 Elsevier Inc. All rights reserved.
doi:10.1016/j.jcp.2007.02.029

analytically [5], and recently numerically [6]. A hollow electron column with axial mirrors has also been considered [7]. Penning–Malmberg traps have been recently used in experiments for the production of anti-hydrogen [8,9] and are being considered, with mirror fields added, for future experiments to confine the anti-hydrogen itself [10,11]. Recently, the effects of a multipole magnetic field intended to trap the anti-hydrogen radially in such a trap have been studied experimentally [12], theoretically [13], and with simulations [14]. Numerical simulations of a plasma in a trap with additional elements can play a major role in clarifying the properties of the equilibria in a complex 3-D configuration, which are as yet poorly understood, and in illuminating the transport properties of such plasmas.

Particles in non-neutral traps performs several types of motions. They gyrate rapidly around the field lines in a high magnetic field. They also oscillate axially between the regions within the confining electrode rings. The bounce time is typically much longer than the gyroperiod. In addition, the particles perform a slow $\mathbf{E}\times\mathbf{B}$ rotational drift. This drift is a consequence of the self and applied fields. The rotation causes particles to cross-field lines on a yet slower time scale. On a slower scale still, collisions drive the system toward equilibrium. In many experimental situations, studies of equilibrium plasma and the approach thereto are performed by applying time varying fields and measuring the plasma response. Detailed comparisons, therefore, require initial plasma that is a good model of the equilibrium in the experiment. Thus, obtaining a robust computational equilibrium for the plasma even before the application of the time varying field is essential for the analysis of such systems.

A schematic of a Penning–Malmberg trap with additional confining elements including mirror coils and quadrupole magnetic field for neutral particle confinement is shown in Fig. 1. In an actual experimental trap, electrons are injected from a negatively biased cathode, enter the confinement region, and reflect from the negative potential at the far end of the trap.

The plasma is created when electrons are trapped as the voltage is changed on a nearby gate. The electrons enter the system with energies of a few eV and, if the walls are cold, may subsequently cool (via synchrotron radiation) to the wall temperature. In a simulation, a method based on first principles would require simulation of the injection from the cathode, and the subsequent approach to equilibrium via synchrotron cooling. However, such an approach appears to be impractical on current computers (even supercomputers) using standard simulation methods, if the actual processes and their associated time scales are to be captured accurately. In a similar approach (but without synchrotron cooling), phase-mixing arising due to the numerical collisions in a particle-in-cell (PIC) code, would eventually drive the trapped plasma to an equilibrium; however, the characteristics of such an equilibrium may might differ substantially from those of the one equilibrium that is reached experimentally.

An alternative is to start the simulation either from an arbitrary plasma distribution or from a prescribed idealized equilibrium state. We have performed studies of the evolution of distributions with initial Gaussian longitudinal velocity distributions, and with a variety of (arbitrary) plasma densities. These studies show that the plasma evolves, via halo formation, to phase-mixed equilibrium that are, as described in Appendix B, near to the corresponding idealized distribution. However, even a straightforward loading of an idealized equilibrium does not, unfortunately, correspond to a computational equilibrium and the distribution may distort, becoming noisy and deviating from the original equilibrium. Without special coding, realistic collisions are not present in a PIC code. Furthermore, it is not clear, even if one were to successfully obtain a computational equilibrium, that this equilibrium would be maintained when parameters of the system are slowly varied.

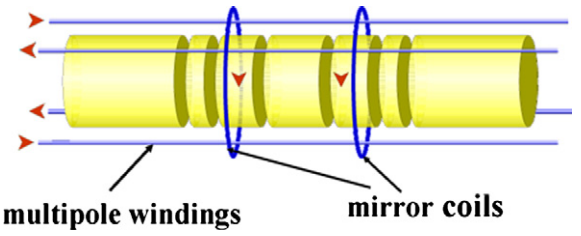

Fig. 1. Schematic figure of a Penning–Malmberg trap with additional multipole fields and mirror coils. Such a trap is being considered for anti-hydrogen production experiments.

Nonetheless, it is important to obtain a tool that enables computing the equilibrium in the trap of the non-neutral plasma with specific electrostatic and magnetic fields at a definite temperature, especially if the analytical specification of the equilibrium configuration is not available or achievable. In the present paper, we demonstrate a method for obtaining and maintaining a desired equilibrium (at a particular temperature), without the use of "real" collisions in the simulations. Furthermore, we also show that by employing slow changes of the system parameters, new equilibria can be obtained. We shall see how numerical noise, especially which coming from voids in the macroparticle distribution, can be exploited to enable the achievement of a computational equilibrium in an efficient manner.

These ideas are illustrated for experimental parameters and configurations that are relevant to the problem of positron confinement in anti-hydrogen traps. The detailed study of positron confinement is presented in [14]. The simulations were done for geometry close to that of an experiment conducted at UC Berkeley [15] as part of the ALPHA [10,11] collaboration. The suggested scheme to trap the anti-hydrogen constituents (positrons and anti-protons) as well as the newly formed anti-hydrogen itself is the addition of multipole magnetic fields to a conventional Malmberg–Penning trap. The equilibrium of a conventional trap without multipole fields has been widely studied, and its local equilibrium solution can be obtained by other means [16]; however, characterization of the system in the presence of the multipole fields is still a subject of research.

The simulation of proposed cold anti-hydrogen traps involves a wide range of spatial and temporal scales, complicating the numerical modeling. We will not concentrate on all the simulation difficulties for the full physical description of anti-hydrogen traps, detailed in [14]. For the present study, the axial magnetic field is about 1 T, corresponding to cyclotron frequencies of the order of tens of GHz, while the multipole fields are varied on an approximately 1-s timescale. While such a range of time scales is impractical to simulate with the current tools, WARP simulations are performed for times longer than the $\mathbf{E} \times \mathbf{B}$ rotation period. For faster convergence, it is important to begin the multipole ramping with a realistic equilibrium plasma (a good "first guess"). Our new method allows for the study of ramping multipole fields and comparing trapped populations for various system parameters.

The mirror coils used to trap the neutral particles axially are not simulated here. However, we have used [6] the same technique described here to confirm previous analytical models [5] for the equilibrium of non-neutral plasma in a Penning–Malmberg trap with a mirror field [6].

It is important here to note, that since the equilibria with a multipole field in the anti-hydrogen trap is unknown and subject of research, the validity of our scheme is ensured only partially by comparing the results of our simulations to the experimental data, since detailed information on the charged particles equilibria in those traps is still not available. In fact, latest experiments of the ALPHA collaboration [17] have shown that indeed the plasma in an anti-hydrogen trap behave as can be deduced from our simulations, and in fact octupole magnetic field for the trapping of neutral particles traps permits better confinement of the plasma whereas quadrupolar fields would not. However, there are more direct indications which ensure the validity of our procedure for obtaining equilibrium: First, the same scheme applied on the trap with mirror field [6] leads to the analytically expected equilibria [5] with its peculiar features typical to the non-neutral plasma. Second, our procedure leads to a numerical equilibrium even before the application of the extra trap elements which is the same as the idealized one with which we load the simulation.

We describe in the present work the various methods that were considered in order to obtain the desired computational equilibrium. Only one suggested scheme led us to the desired result, and it is this method on which we concentrate. However, the other schemes contributed to our understanding of the process of reaching a computational equilibrium, and therefore are also presented in the Appendix.

The paper is organized as follows. In Section 2, we describe the procedure to obtain the desired equilibrium. In Section 3, we show the results of simulations initiated using a nominal equilibrium, for the case of an anti-hydrogen trap. These results may be contrasted with the results of injection simulations, shown in Appendix A. In Section 3.1, we present the geometry and parameters. In Section 3.2, we present the results. We show how a quiescent r–z idealized equilibrium profile can be realized in a simulation (Section 3.2.1), and how a 3-D equilibrium with additional elements is obtained (Section 3.2.2). In Section 3.2.3, we present a computational study showing in detail how the relaxation process depends on different parameters of the simulation. In Section 4, results of alternative considered schemes are discussed. A discussion is given in Section 5. In Appendix B, we investigate the evolution of a non-equilibrium profile that initially has a Gaussian longi-

tudinal velocity distribution. We describe the equilibrium to which the simulation relaxes as a result of phase mixing and numerical effects.

2. Quiescent numerical equilibrium via a multi-stage relaxation procedure

The new procedure developed for generating a quiescent numerical equilibrium distribution follows a multi-stage approach. Starting from an idealized approximation of the equilibrium configuration in a coarse representation at lower dimensionality, the numerical parameters are slowly (almost adiabatically) modified toward a detailed solution of the full three-dimensional configuration. The successive stages are summarized as follows:

1. Load large-weight macro-particles with a two-dimensional r–z idealized equilibrium profile (which is solved separately [16]).
   The initial number of macro-particles per cell is typically of the order of unity or less, so that the amplitude of typical axial oscillations that exist in the vicinity of equilibrium (described later in more detail), as well as the oscillations in their RMS decreases fast (relatively small number of time steps), thanks to a high level of numerical collisions.
2. Evolve the simulation with the r–z solver, using a relatively large time step, until a computational equilibrium is reached.
   Typically, the small axial oscillations have reduced their amplitude by a factor larger than two, and the RMS oscillations by a much larger factor.
3. Gradually increase the number of macro-particles until numerical noise is reduced to an adequately small level.
   The number of particles can be increased by a factor of two or three (by simple splitting) to the desired fine resolution level required for a simulation in cylindrical geometry. Before each gradual change the axial oscillations and their RMS variations decrease as in the previous step.
4. Switch to the three-dimensional field solver and run until a new equilibrium is reached. In this stage we can proceed by further gradual increase of the macroparticles number while slowly relaxing the solution to a 3-D computational equilibrium.
   The relaxation to the 3-D equilibrium is done with the same control procedure of the plasma oscillations as the previous steps.
5. Decrease the time-step toward a fraction of the characteristic time scale, so that it is small enough for modeling the system evolution when system parameters (for example, multipole strength) are changed.
6. Slowly, turn on additional physics (in our case, external multipole field).
   The slow ramping of any additional element satisfies a slow enough variation in time such that any important physical effect, such as particles axial bounces time, is faster that its variation.

The use of large-weight macro-particles in stage 1, in order to obtain high numerical noise, and the use of large time steps (stages 1–4), are both aimed at obtaining rapid computational relaxation toward temporary and approximate equilibria. This is an essential prerequisite for the simulation studies of the stability and transport properties of trapped non-neutral plasmas, as we aim to. Note that using a "conventional" scheme, in which high resolution is applied from the beginning, leads to time scales for reaching an equilibrium state, which are too long in practice. In fact the decay of the axial oscillations and the smoothing of the fields were not reached within a reasonable time, when trying the conventional method.

3. Simulation description and results

All of the simulations presented in the present paper (and in [14]) are done with the WARP code [18], designed originally for heavy ion beam simulations. This is a 3-D PIC code that considers the self-electrostatic fields of the particles, together with those of external magnetic and electric elements. WARP was chosen as the simulation tool because it has many useful features for the study of non-neutral plasmas in traps. For example, traps often confine strongly magnetized plasmas, wherein the particle motion is nearly a guiding center motion. In this case, WARP allows the time step to be much larger than the gyro period and still properly

calculates the various drifts and Larmor radius [19]. WARP contains fully three-dimensional field and boundary elements. One other feature used here is the ability to vary the numerical algorithms in use as the run proceeds. For example, WARP can switch from a 2-D field solver to a 3-D solver, and particles can easily be added during the simulation.

3.1. Simulation parameters and geometry

The simulations presented in this paper all have the geometry shown in Fig. 1, which is a schematic of both the UC Berkeley experiment (which was done with a quadrupole field [12]) and the ongoing ALPHA experiment (done with an octupole field [15]). The code model included the trap conductor wall, axial voltage rings and ramped multipole magnetic fields. The trap mirror coils which are shown in the figure are not included in the simulations presented here. Their effect has been the subject of a separate study using the same methods as the one presented in the present paper, and will be discussed elsewhere. Following the experimental parameters in [15], we assume a solenoidal field of $B_0 = 1$ T, a maximum magnetic field strength of the multipole given by the wall value $B_w = 1.7B_0$, and a wall radius $r_w = 2.3$ cm. The initial radius of the plasma column is R_p and the plasma length is approximately 6 cm (the exact length depends on the particle velocities, radial positions and trapping electrode voltages). In the injection simulations, the trapping electrodes have a length of 2 cm, and the cathode is at 5 V. The far electrode is held at 100 V and the boundary beyond is grounded. In the equilibrium simulations we use Neumann boundary conditions axially and each trapping electrode has length 3 cm and is at 100 V. For both types of simulations, the central electrode is at ground (at $r = 2.3$ cm). The plasma density is in the range of 10^6–10^7 cm^{-3}.

The grid spacing (unless stated differently) is $\Delta x, \Delta y, \Delta z = 1$ mm, and the time step size is $\Delta t = 10^{-10}$ s. This time step size encompasses a few gyration periods of the positrons, and thus the novel WARP particle pusher [18], that allows use of large time steps while preserving the correct gyroradii, is used.

The number of simulation particles ranged between 10^5 and 10^6 (depending on the initial plasma column size), and there were about 40–70 real particles per macro-particle. The number of macro-particles per cell varied from a few to several tens. In the injection simulations presented in the Appendix, positrons are injected toward the interior of the cylindrical trap from the cathode.

3.2. Results

We present results from the application of the new procedure to the modeling of the anti-hydrogen trap. The idealized phase-space distribution function satisfies the time-independent Vlasov–Poisson equations with a Boltzmann factor (as discussed in [16]). The velocity distribution is Gaussian, and the corresponding density profile, before the multipole is ramped, is such that along each field line, the external electrostatic field when superimposed with the self-field produces a constant potential inside the plasma. The plasma density is constant along the axial magnetic field lines in the edge region, which is of order one Debye length in extent. Thus, there is freedom in the total charge along each field line. In Fig. 2, we show two self-consistent equilibrium density profiles that were obtained by solving the Poisson equation assuming a Boltzmann distribution for the particles. The positron temperature was assumed to be 1 eV. The maximum density is about 2×10^7 cm^{-3}.

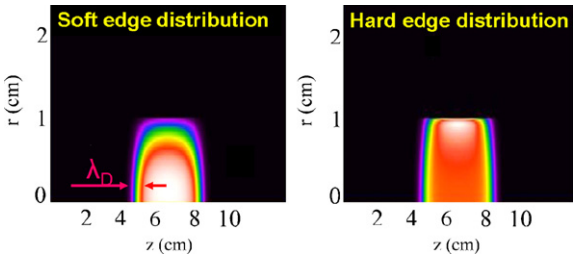

Fig. 2. Two possible equilibria are shown: (left) "soft edge", with a radial decrease of net line charge toward the plasma edge; and (right) "hard edge", with constant net line charge.

3.2.1. R–Z equilibrium (stages 1–3)

An idealized equilibrium was loaded into WARP by seeding macro-particles with the idealized density distribution, with a velocity spread corresponding to the chosen temperature. The chosen initial distribution was that of the soft edge density profile given in Fig. 2. The time step in this stage may be larger than the used one when the additional elements are added (step 6), and in this case was $\Delta t = 10^{-9}$ s.

In Fig. 3, we show results before numerical equilibrium is reached, and after. The initial density profile is not smooth but, after relaxation and macroparticle multiplication (stages 2 and 3, respectively), the density profile has become a very smooth Gaussian, and the density profile more closely resembles the initial density profile data, as can be observed directly by comparing with Fig. 2 (soft edge case). The time history of the mean axial velocity and its RMS are shown in Fig. 4. We observe that the axial velocity exhibits oscillations that eventually damp out and the final velocity spread is very close to the initial, corresponding to a little less than 1 eV. These are typical oscillations that appear when the simulation nears equilibrium. In Appendix B, the same procedure steps 2 and 3 are applied for a case of an initial arbitrary density profile (as opposed to step 1) and also in this case axial oscillations appear when equilibrium is approximately reached.

3.2.2. Toward 3-D equilibrium (stages 4–6)

We now proceeds by showing how the 3-D equilibrium simulations are done, to achieve our main purpose: the calculation of an unknown equilibrium under the presence of additional elements. In the antihydrogen trap case, the new element is a multipole magnetic field and the effect of this field on equilibrium positron configurations is a main subject of interest. These are the so-called equilibrium simulations that we presented in detail in [14]. Result of such an equilibrium simulation are shown in Appendix A and illustrated in Fig. 5. In the same appendix, the equilibrium results are contrasted with results of injection simulations showing the very different plasma distributions obtained in each case.

Such simulations are done as follows: we continue the simulation from the stage shown in the previous subsection, which is an r–z simulation that evolves to equilibrium (see Figs. 3 and 4). When r–z computational equilibrium is approximately reached we switch to the 3-D solver (step 4), which causes again a significant disturbance in the equilibrium. However, here we also follow the same procedure as in the r–z solver, which was described in the previous section, namely relaxing to equilibrium and gradually increasing the number of particles. As we shall see in Section 3.2.3, such increase of particles alone (i.e., increase of macroparticle numbers along with reduction of weight) does not cause a significant change in the process of relaxing to

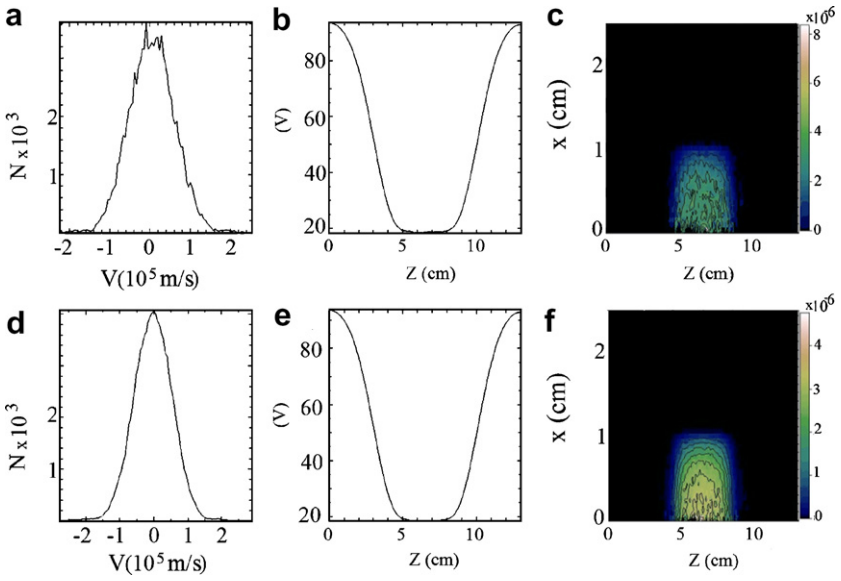

Fig. 3. The initial (top row) and final (bottom row) velocity (speed) distribution function (a and d), variation with z of the on-axis (b–e), electrostatic field, and density distribution (c and f), for a simulation initialized with an idealized soft edge equilibrium (as shown in Fig. 2).

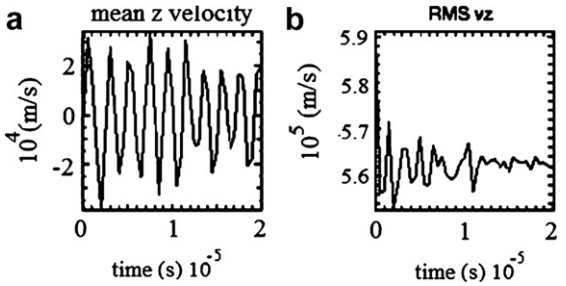

Fig. 4. The mean axial velocity and it's RMS as functions of time.

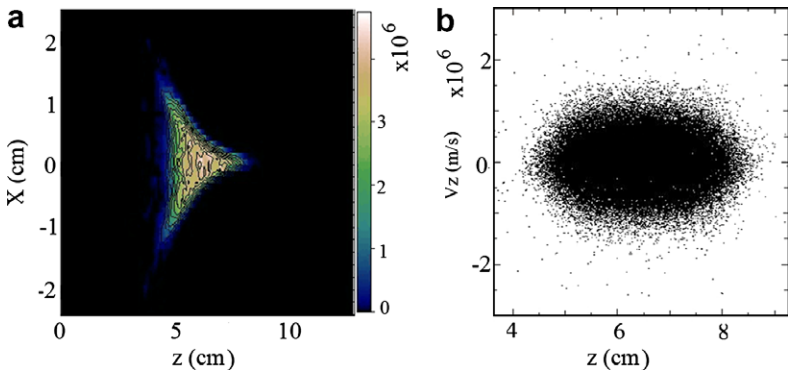

Fig. 5. Equilibrium simulation for the case of a quadrupole field, after the field has reached its maximal value. The initial radius of the plasma column, r_p, was 10 mm. Panel (a) is the density in z–x-plane, and (b) the axial velocity phase space.

equilibrium. Only when the equilibrium is closely reached do we decrease the time step to 1×10^{-10} s and slowly turn on the multipole field.

3.2.3. Characterization of the relaxation to equilibrium through stages (stages 2–6)

We now proceed by studying the effects of increasing particle number, switching to the 3-D solver, changing the grid size, etc., on the process of relaxation to equilibrium. We do this by characterizing the axial oscillations while performing steps 2–6.

In Figs. 6a–c and 7, we show a series of plots similar to those in Fig. 4 and in Fig. 8 presented in Appendix B (in which steps 2 and 3 are applied to the non-equilibrium initial profile as discussed in Section 4). The relaxation to computational equilibrium includes axial oscillations that damp out. The oscillations are longitudinal, since the field lines are initially purely axial and the particle motion is constrained to the field lines. These oscillations appear to be due to the finite grid spacing, as we shall see from the following discussion. We now characterize these oscillations and show that their amplitude is larger for smaller Debye length (which adds to the complexity of plasmas with small Debye length). They are damped as the plasma is heated and the Debye length increases. Thus, when there are fewer particles per cell and more numerical noise the equilibrium is approached more rapidly. Fig. 6 shows the equilibration process during such a procedure for three different cases of initial particle number and grid cell size. The cases with differing numbers of particles, and the same grid cell size, measure the effect of numerical heating, while the cases with differing grid cell sizes are such that the number of particles per cell is kept constant. The plasma is started with an initial column of 1.2 cm and an octupole multipole field is applied. The densities are somewhat higher than in the 1 cm plasma column of Section 3.2.1. Note that in the following examples we only illustrate the effects of changing parameters in the procedure and therefore in order to have a shorter simulation, we did not wait in each step to relax to a quiescent state. In the full equilibrium simulations we choose proper times for each step so that a quiescent result is obtained before each change (i.e., switching to 3-D, multipole ramping, etc.)

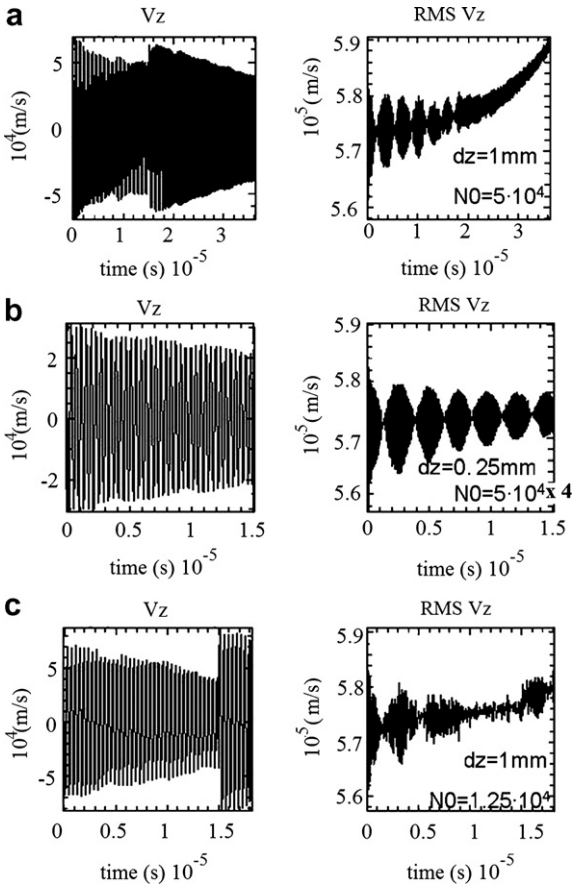

Fig. 6. The mean axial velocity and its RMS as a function of time for three cases: (a) $\Delta z = 1$ mm and initial number of particles $N_0 = 50{,}000$; (b) $\Delta z = 0.25$ mm and $N_0 = 200{,}000$; (c) $\Delta z = 1$ mm and initial number of particles.

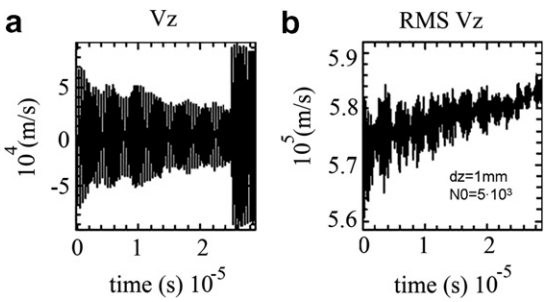

Fig. 7. The mean axial velocity and its RMS as a function of time for $\Delta z = 1$ mm and initial number of particles = 5000. The number of particles is multiplied at $t = 1.5 \times 10^{-5}$ s.

In cases shown in Fig. 6a–c, the 3-D solver is switched on at time 1.5×10^{-5} s. In Fig. 6a, the histories include times where the multipole has been turned on (at time $t = 2 \times 10^{-5}$ s). This is the cause of the fast increase of the V_z RMS starting at that time-particles are moving toward the wall, and the simulation does not indicate particle heating in this stage. We change Δz or the number of particles per cell (leaving the grid unchanged), in the various cases. We see how the relaxation to equilibrium is affected by the details of the procedure used.

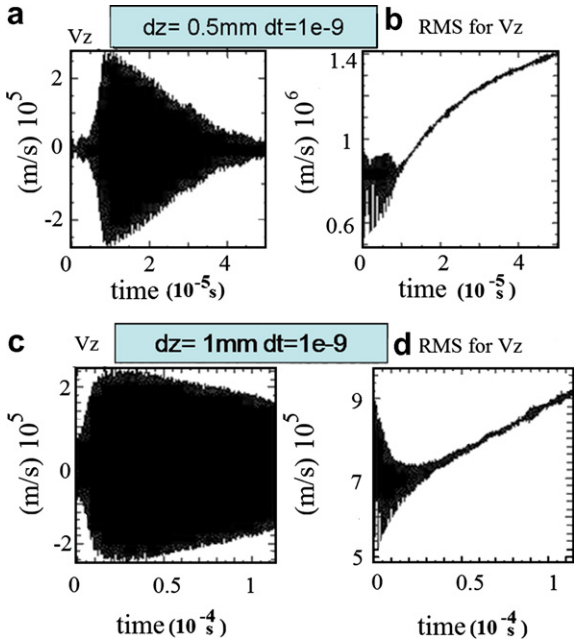

Fig. 8. Mean and RMS of axial velocity as functions of time, for the simulations presented in panels (a) and (c) of Fig. 13. The former shows particle loss; in the latter, the problem was solved by use of a larger Δz.

When Δz is smaller, the initial velocity is smaller, but if we keep the number of particles per cell the same, the decay of these oscillations is the same and we observe that the heating is also the same. The decay of the oscillations is closely related to the numerical heating, and it is faster for the larger heating that occurs with fewer particles per cell. The velocity is also smaller for a larger Debye length or for lower density plasmas: Figs. 6 and 7 can be compared with Fig. 4 (with lower density) or with Fig. 8b (for very high density cases). One can observe that the oscillations are about an order of magnitude larger for the very dense cases. This again shows the complexity of simulating cases with very small Debye length. When we permit large numerical heating by taking a smaller fraction of the initial number of particles, the initial velocity does not change, but the decay of the oscillations is much faster.

In Fig. 9, we show a graph of the maximum of the initial amplitude of the oscillating velocity as a function of the grid cell size (the number of particles per cell is kept constant). We see that for larger Δz the behavior is close to being linear. Apparently for small Δz, the behavior changes – so that for $\Delta z \to 0$ (impossible to actually simulate) we may expect that the oscillations would disappear.

In all these simulations, except the one in Fig. 7, the initial number of particles (in the r–z mesh) is doubled at 0.2×10^{-5} and tripled at time 1.5×10^{-5}, at the same time that the solver is switched to 3-D (the number of particles per cell is still lower in the 3-D solver case than in the 2-D). In Fig. 7, the number of particles is dou-

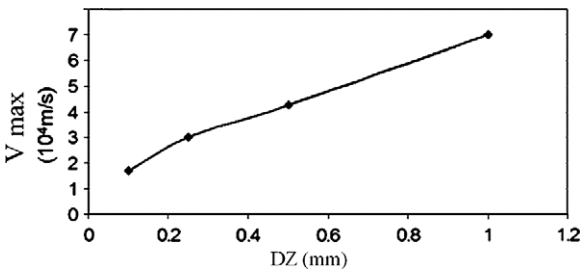

Fig. 9. The maximum axial velocity as a function of Δz, holding the number of particles per cell constant.

bled at 0.2×10^{-5}, but it is multiplied by 4 at 1.5×10^{-5} s and by 5 at 2×10^{-5} s. The switch to 3-D is done at 2.5×10^{-5} s, Δt is decreased at 2.8×10^{-5} s and the multipole is turned on at 3×10^{-5} s. In this simulation the heating is the largest since we used a very small number of particles initially. We can see that the change in the number of particles does not introduce any discontinuities in the solution, but the passage to 3-D does. This passage is more discontinuous for cases with smaller Debye length. Since a change in the number of particles does not introduce disturbances, we can again increase the number of particles after the 3-D equilibrium is reached, just before the multipole field is turned on. This field is ramped slowly, so that it does not introduce an abrupt disturbance (we have used the same procedure in order to study the effects of the mirror field). The equilibrium found is as expected from analytical estimates [6].

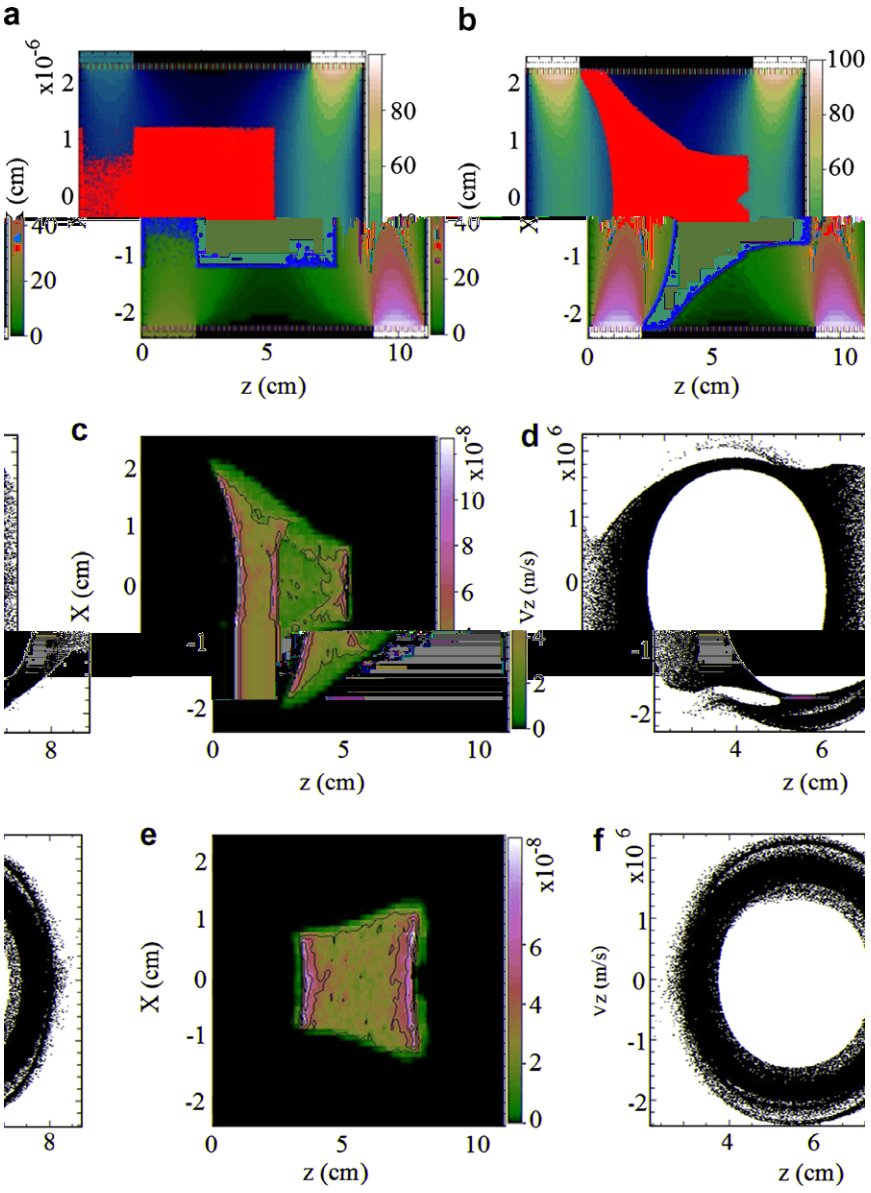

Fig. 10. (a) Geometry of injection simulations. The color map shows the electrostatic potential and red dots represent the positrons; (b) particles integrated over the perpendicular coordinate y. The ballistic charge loss at the walls under the influence of a quadrupole magnetic field is observed, at time 0.7 μs and with $r_p = 12$ mm; (c) charge density in the x–z-plane at the same time; (d) phase space (axial velocity versus axial coordinate) at the same time; (e) charge density for an octupole case (at time 3 μs); and (f) phase space of octupole case at the same time.

4. Comparison to other attempted procedures

Various other schemes for initializing such an idealized computational distribution in the simulation were attempted. For example, injecting a plasma, such as shown in Appendix A, leads to some phase mixing and a final distribution that is quasi-static. This distribution is, however, far from the idealized case. The injected plasma has particles streaming in both directions, initially at a fixed velocity, and slow particles only at the plasma edges. This longitudinal phase space does not differ much from those shown in Fig. 10. In some cases (see Fig. 11), the phase space may fill rapidly if instability occurs. The rich dynamics of injection were studied in [20].

Another possibility is to load a prescribed distribution in the trap center and allow it to evolve to a steady-state, using the techniques discussed above (e.g., adjusting the time step and slowly increasing the particle number, etc.). For example, we started with a cigar shaped initial profile, with a Gaussian velocity distribution and a top-hat transverse spatial distribution. With such a procedure the plasma evolves to a state close to an idealized equilibrium, except for a noticeable halo and concomitant tail in the velocity distribution. This halo is the source for a numerical instability, as described in Appendix B.

The fact that we have shown that equilibrium can almost be reached by this procedure (starting from a non-equilibrium profile, and relatively far from the equilibrium state), enables us to confidently calculate the equilibria with multipole fields and expect that the particle configuration obtained during multipole ramping is in fact the proper one, such as the results shown in Fig. 5.

As computational equilibrium is being reached; the plasma exhibits axial oscillations that slowly decay. These oscillations are larger as the grid size is larger and are related to the Debye length of the plasma. For larger Debye lengths, the oscillations are smaller. We conclude that we require grid cells small enough to resolve some fraction of the Debye length, in order to obtain a relatively slow axial motion. However, since there is numerical heating that eventually leads to a larger Debye length, the oscillations slowly decay.

5. Discussion

We have developed a method for obtaining an equilibrium in PIC simulations for non-neutral plasmas within a confining trap, taking advantage of the artificial numerical collisional heating in the PIC code (which

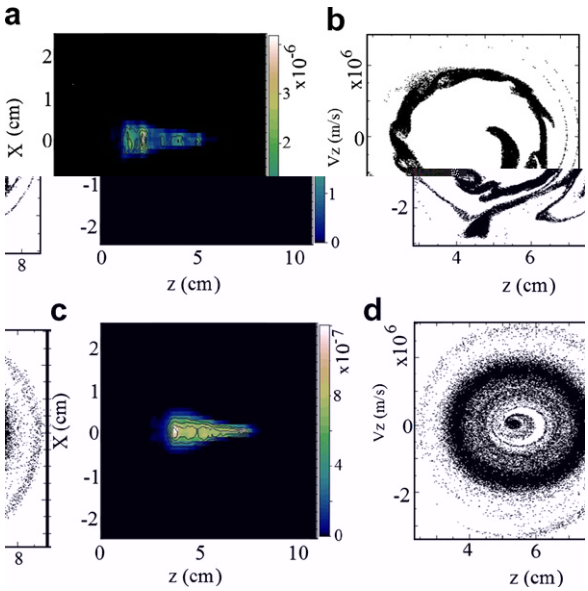

Fig. 11. Injection simulation in a case that exhibits instability, for initial plasma radius of $r_p = 2$ mm and with a magnetic quadrupole. (a) Density at z–x-plane at 0.7 μs (b) axial velocity phase space at the same time as in (a). (c) Density at z–x-plane at 3 μs and (d) axial velocity phase space at the same time as in (c).

does not necessarily model realistic collisions). The traps can include several electrostatic and magnetic field elements. An underlying assumption is that there is a high magnetic field confining the plasma. We have illustrated suggested methods for obtaining a suitable equilibrium in simulations of an antihydrogen trap, including discussion of specific numerical issues.

We also discussed the features of WARP that make it suitable for such simulations, such as the drift kinetic particle mover and the ''steerability'' of the code.

The method that we described requires a priori knowledge of the equilibrium of the trap in the absence of the slowly ramped multipole field elements. With this scheme, we use the numerical collisionality in order to reach a robust computational equilibrium from the initially loaded nominal equilibrium density profile. We show that solutions can relax to the loaded equilibrium and maintain it. A major outcome is that, with this computational equilibrium, we can proceed to find unknown equilibria in the presence of external fields. We observe fast oscillations as the computational equilibrium is approached, but these are also damped by using our scheme. There are several numerical difficulties in obtaining computational equilibrium. The Debye length has to be resolved over several grid cells. This is a major problem in modeling cold or very dense plasmas. It may be that the use of time-implicit PIC methods would relax this restriction, but (since important physics often occurs on the Debye length scale), further study would be needed.

Other considered methods for obtaining equilibria are discussed in the Appendices. Appendix A describes an ab initio method whereby the plasma is formed directly by injection from the source. Appendix B describes a method where an arbitrary initial density profile is loaded and allowed to relax toward equilibrium. In their present form, these other methods do not lead to the required equilibrium and have not proven useful. However, it may be possible to develop improved schemes that will allow reaching a desired equilibrium from a more casually chosen initial configuration. Such methods could include a numerical model for a damping term [21–23], numerically added synchrotron radiation, etc. However, all these should be carefully studied, and any method will require that care be taken so that the desired equilibrium temperature is approximately maintained as the calculation evolves.

Acknowledgment

This work has been supported by US DOE division of High Energy Physics, Grant No. DE-FG02-04ER41289 and was partially supported by the ISF (Israel).

Appendix A. Comparison between equilibrium and injection simulations

We here shows the results of an equilibrium simulation done with the new method and compares it with the results of injection runs. We stress that the obtained results describes a local equilibrium along field lines – a global equilibrium would be reached only for longer simulations with much higher numerical noise. However, we are interested in local equilibrium, as this is physical situation in many of trapping experiments.

For a practical trap parameters with a quadrupolar magnetic field there is a dramatic ballistic loss of positrons, as predicted [13], shown in experiment [12], and simulated [14]. Usually the multipole is ramped over few seconds, requiring an equilibrium simulation to describe the processes involved. At the time that the multipole reaches it's maximum, a very small fraction of the original particles remain in the simulation. This fraction corresponds to the number of particles in a plasma column of radius of a critical radius [14]. According to the simulations in [14], in order to prevent this ballistic loss an octupole magnetic field instead of a quadrupole magnetic field can be used [14]. For an octupole, the critical radius is much larger than that of a quadrupole. This was also recently confirmed experimentally [17].

In Fig. 8, we show the result of an equilibrium simulation obtained by the scheme described in Section 2 at a time where the quadrupole field has reached its maximum. The plasma density in that simulation was, as in the previous section, $1–2 \times 10^7$ l/cm^3, the positron temperature is 1 eV, and the initial plasma radius, r_p, is 1 cm. The initial plasma radius was 10 mm and most particles have been lost. In this case the constant density lines approximately follow the field lines of the maximal value of the multipole ramp.

Fig. 10, shows a typical injection simulation for the cases of quadrupole and octupole magnetic fields. This is in part to show the ballistic loss process, which is important for our example that is evident either in equi-

librium simulations or in injections simulations. However, the main reason for showing these results is to emphasize the differences with equilibrium simulations. Fig. 10a shows the plasma as it is injected into the trap. The potential is shown with a color map and one can clearly see the voltage of the electrodes. Macroparticles appear as red dots. In Fig. 10b, the particles are shown for a quadrupole case at a time where the quadrupole field has not yet reached its maximum. One can observe the dramatic loss of particles. In Fig. 10c, the corresponding density is shown. Here density oscillations (which have typical time scales of 10–100 ns) are observed. These oscillations are not present in an equilibrium run. In Fig. 10d, the axial velocity phase space is shown. One can see that the velocity distribution is far from the expected equilibrium, namely, a Gaussian (centered at the origin). The hole in phase space does not fill up for very long simulations nor when very few particles are simulated (thus with increased numerical noise). One could consider adding a model of synchrotron radiation, which will necessarily lead to a significant change of the phase space; however, this will lead to a slowly varying equilibrium with a varying temperature, and perhaps a non-uniform temperature. This is certainly a physical process that can be important in some systems including the anti-hydrogen case. However, in the present study we are looking for a method that permits establishing definite temperature equilibrium. In Fig. 10e, we show the density profile for a case with an octupole at a time after the multipole reached its maximal value. One can see the large number of particles that still remain in the simulation. In Fig. 10f, the phase space is shown.

The injection simulations show the existence of highly nonlinear longitudinal phase space dynamics [20], which are not typical for equilibrium simulations. In Fig. 11, we show one example that occurs independently of the magnetic multipole and appears in long narrow initial plasma columns. We see that the instability leads to a phase space which does fill out. It may be possible to reach the required equilibrium from such an injection simulation by adding high numerical noise. The instability, however, appears only for some parameters.

The results of the equilibrium simulations are quite different from the injection simulations. The phase space of the equilibrium simulation is a Gaussian, while the phase space of the injection simulation reaches a steady state with a hole inside (Fig. 10), unless some instability arises (Fig. 11). In both figures, Figs. 10e and 11c, the plasma oscillations (which are typical of the injection simulations, as opposed to the equilibrium ones) that are evident in Fig. 10c is already damped, reaching a steady state density profile that can be a typical equilibrium for an injection process. This equilibrium is very different from the equilibrium density profile obtained with our method. One can see that in the injection runs the density, for example, is higher towards both axial boundaries of the plasma, while in the equilibrium simulations the density is highest inside the plasma, and on its boundary there is a gradual increase of the density over a distance of the order of the Debye length.

Appendix B. Simulations starting from a non-equilibrium initial distribution with a longitudinal Gaussian profile

In Section 2, we discussed the suggested scheme for obtaining equilibrium by using a high level of numerical noise. The initial particle loading scheme has consequences for the results. For example, when particles are injected followed by our scheme increasing gradually the number of particles, large time steps, etc. in order to obtain increased numerical noise, we do not obtain the idealized computational equilibrium. However, if the initial distribution has a Gaussian distribution in velocity, and still is quite arbitrary in space, a closer result to a computational equilibrium is reached by proceeding with steps 2 and 3 of the procedure of Section 2. The importance of this study relies on the fact that, although we encounter some problems (primarily a halo), it is shown that even when the initial plasma distribution is far from the idealized equilibrium, the suggested scheme does result in the computational equilibrium. This has implications for the possibility of obtaining a new equilibrium when some external elements are added to a simulation that is initially in an idealized computational equilibrium. But also it shows that it is not possible to simulate an idealized computational numerical equilibrium properly by only relying on numerical collisions.

In the following simulations, both voltage rings are turned on at the start of the run, with 100 V. Particles are loaded into the trap region with some specific configuration predefined in WARP. The particles are loaded with a "cigar" shaped profile (with parabolic fall-off in the line-charge density in the ends of the plasma) and with a uniform transverse distribution (this should lead to an equilibrium which is more similar to the hard edge one shown in Fig. 2) The longitudinal velocity spread is about 10^6 m/s (which is about 2.5 eV in temper-

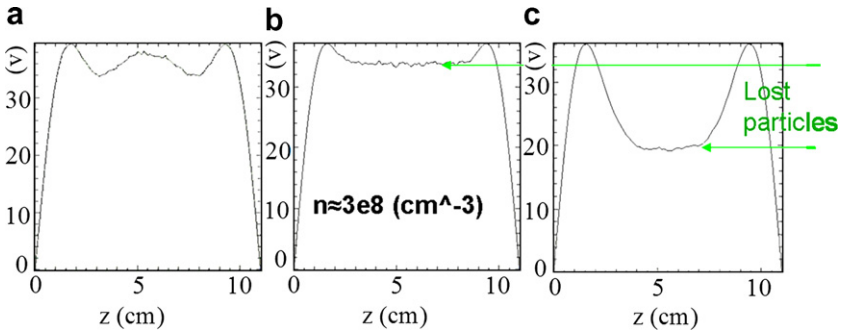

Fig. 12. The electrostatic potential in the axis at three simulation times: 0.02×10^{-6}, 0.64×10^{-6}, 80×10^{-6} s for density 3×10^8 cm^{-3}.

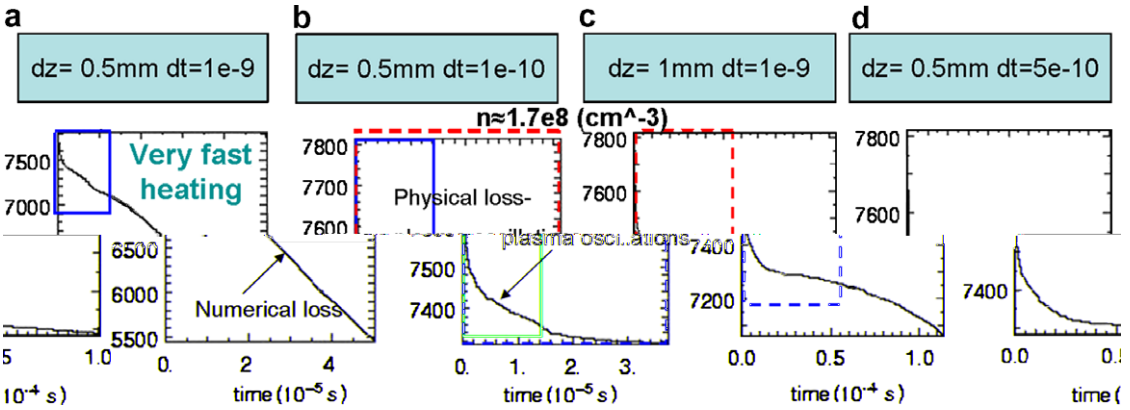

Fig. 13. Number of particles versus time for four simulations with different longitudinal grid spacing Δz and time step size Δt, as indicated in the box in each panel. The blue and red boxes denote regions with similar behavior for the same time scales. (For interpretation of the references to colour in this figure legend, the reader is referred to the web version of this article.)

ature). We show a simulation in which we followed the scheme of high numerical noise, with a quite large density of 3×10^8 cm^{-3}. We use this large density to better illustrate the problems encountered. The plasma length and density are arbitrary. In the present example, the plasma is rather narrow with width of 2 mm. In Fig. 12, we show plots of the electrostatic potential on the axis at three different times. These are r–z simulations with a relatively small number of particles and a time step of 10^{-9} s. We see that initially the electrostatic potential is not flat, since we started with a non-equilibrium arbitrary distribution. At 0.64×10^{-6} s the electrostatic potential stabilizes with a quite flat profile, indicating a null net electric field as expected in the idealized equilibrium. This profile is quite steady until the plateau of the electrostatic potential starts to descend, as is seen at $t = 80 \times 10^{-6}$ s in the third panel. This drop is caused by particles escaping the trap axially, and is followed by a density drop. This process continues until all particles escape the simulation.

We have checked that the calculated time-varying plateau corresponds to the idealized equilibrium of the instantaneous density. Therefore, although we do get close to equilibrium results, we have a major problem in these simulations. The cause of this is explained in the following discussion.

In Fig. 13, we show four results for a similar simulation, with the same plasma length, width and initial velocity distribution, but with a lower density, $n = 1.7 \times 10^8$ cm^{-3}, and with different longitudinal grid spacing and time steps. In Fig. 13, the time histories of the number of particles are plotted. The numerical grid and time-step size parameters are indicated for each case. We note that the simulations are run for different times. The blue boxes[1] indicate regions (in time) where their results are similar. We can see that when we consider a

[1] For interpretation of the references to colour in Fig. 13, the reader is referred to the web version of this article.

large time step and time (as in the previous simulation), which is shown in (a), particles are lost very quickly. When analyzing the particles' velocity distribution for this case (Fig. 8a) we can see that at a time of 1×10^{-5} s a very large and rapid particle heating occurs, which is not related to the standard numerical heating, causing particles to escape the trap continuously. When we consider a fine grid in time and space (Fig. 13b), the number of particles decreases initially just as in the first case, and we also observe the same initial particle loss (in the blue box area[1]); however, as opposed to the previous case, the number of particles stabilizes. In this case (b) the number of particles per cell is the same as in (a), but the heating is much slower. Here there is a normal degree of numerical heating, saturating at 2×10^{-5} s.

The initial particle loss that is indicated in the blue box[1] is the same as that inside the blue box[1] in the previous case, and is due to plasma oscillations. This particle loss changes with the density of the positrons, and occurs since we started from a non-equilibrium profile. Particles can escape axially from the trap due to these oscillations, which is a physical process.

However, the particles in the first case (a) continue to escape the trap due to this very large heating. The source of this very large heating is apparently a numerical instability coming from the fact that there is a large enough number of fast particles. The deviation from the standard heating indicates this numerical instability. The source of this relatively large number of fast particles will be discussed below. Although the bulk of the plasma is slow, and $\Delta z/\Delta t < \Delta v$ for this bulk, this necessary condition for numerical stability is not satisfied for particles in the tail of the distribution function.

The solution for this problem, without reducing the time step, would be to increase the Δz, as is done in the third panel (Fig. 13c). The dashed box indicates the same behavior in this case and in the second case (b). We see that for the same time scales as in the second case the number of particles stabilized, eliminating the particle loss seen in the first figure. The heating rate is exactly the same as in the previous case and can be observed in the lower part of Fig. 8. We note that the time axes for cases (a) and (b) of that figure differ. The heating of the lower case is much slower and the heating is lower. Actually this is the standard numerical heating, which increases with the number of time steps but decreases with the time step size, leaving the heating rate invariant. At larger time steps there is enough heating of the fast particles and the instability occurs again. The forth case (c) shows a situation where no nonphysical particle loss occurs over a large time for quite a large time step.

However, the problem of reaching equilibrium is even more complicated for cases where the Debye length is small relative to the grid spacing. Δz cannot be increased any further, since the Debye length would not be resolved and we would get a numerical instability. In the above example the plasma is nonuniform and the

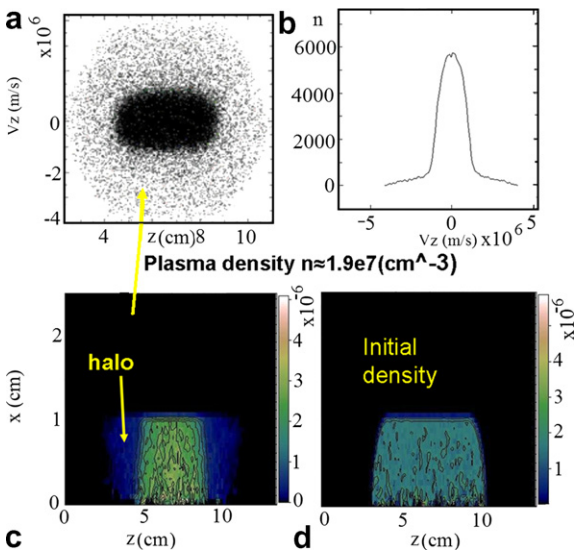

Fig. 14. Simulation for an initially cigar shaped, wide positron column, $r_p = 1$ cm, and large numerical noise. The halo is clearly seen. (a) The longitudinal phase space, (b) the final axial velocity distribution function, (c) the final plasma density, and (d) the initial density distribution of the same system.

Debye length ranges from 0.7 to 1.5 mm. Thus, in the cases shown in Fig. 13 the grid marginally resolves the Debye length, and Δz cannot be larger.

When a plasma configuration starts approaching the computational equilibrium profile; the plasma starts to exhibit oscillations as a whole, see Fig. 8. In Section 3, we started close to equilibrium, and therefore the oscillations in those cases appeared early in the simulation; however, in this case they appear later, as equilibrium is approached. A further discussion in these oscillations is given in Section 3.2.3.

We now clarify the reason for the relatively large number of very fast particles by showing a case with a wide plasma column, of $r_p = 1$ cm, with densities close to the experimental ones, $n = 1.9 \times 10^7\,\mathrm{cm}^{-3}$. In Fig. 14, we show the simulation. The initial density profile is an arbitrary cigar-shaped one, and is far from any equilibrium profile, as one can observe in the lower right hand panel of the figure. After the simulation evolves, we see a clear halo in the phase space as well as in the density profile, which indicates a large number of fast particles. The distribution function appears to be composed of two Gaussians, the first with a small temperature that belongs to the bulk of the plasma, and the other one with a larger temperature that belongs to the halo. It is this halo that is causing the numerical instability. The halo appears since we started far from equilibrium and initial plasma oscillations cause its formation, creating two positron populations of different temperature. It may be that the fast oscillations close to equilibrium further separate the plasma into two populations. The lower temperature population approached closely to the required equilibrium profile (which is similar to a separately calculated hard edge density profile shown in Fig. 2b). This, and the evolving potential shape in Fig. 11, indicate that even when starting relatively far from an idealized equilibrium, numerical collisions evolve the plasma configuration close to the computational idealized equilibrium. This makes us more confident that simulations which start with an equilibrium profile with no multipole field will slowly evolve to the new equilibrium with multipole field, if that field is ramped relatively slowly.

However, the halo indicates that we do not succeed in obtaining the exact idealized equilibrium. Therefore, in order to simulate equilibrium runs via a ramping of a magnetic multipole, we choose to start close to an equilibrium distribution.

References

[1] A. Kabantsev, C. Driscoll, Trapped-particle modes and asymmetry-induced transport in single-species plasmas, Phys. Rev. Lett. 89 (2002) 245001.
[2] T.M. O'Neil, C. Driscoll, Transport to thermal equilibrium of a pure electron plasma, Phys. Fluids 22 (1979) 266.
[3] S.A. Prasad, T.M. O'Neil, Finite length thermal equilibria of a pure electron plasma column, Phys. Fluids 22 (1979) 278.
[4] D. Dubin, T.M. O'Neil, Trapped nonneutral plasmas, liquids, and crystals (the thermal equilibrium states), Rev. Mod. Phys. 71 (1999) 87.
[5] J. Fajans, Non-neutral plasma equilibria, trapping, separatrices, and separatrix crossing in magnetic mirrors, Phys. Plasmas 10 (2003) 1209.
[6] K. Gomberoff, J. Fajans, J. Wurtele, A. Friedman, D.P. Grote, R.H. Cohen, J.-L. Vay, Simulation studies of non-neutral plasma equilibria in an electrostatic trap with a magnetic mirror, Phys. Plasmas (2006) (in preparation).
[7] R. Davidson, A. Drobot, C.A. Kapetanakos, Equilibrium and stability of mirror-confined nonneutral *E* layers, Phys. Fluids 16 (1973) 2199.
[8] M. Amoretti, C. Amsler, G. Bonomi, A. Bouchta, P. Bowe, C. Carraro, C.L. Cesar, M. Charlton, M.J.T. Collier, M. Dose, et al., ATHENA collaboration, Production and detection of cold antihydrogen atoms, Nature (London) 419 (2002) 456.
[9] G. Gabrielse, N.S. Bowden, P. Oxley, A. Speck, C.H. Storry, J.N. Tan, M. Wessels, D. Grzonka, W. Oelert, G. Schepers, et al., ATRAP collaboration, Background-Free Observation of Cold Antihydrogen and a Field-Ionization Analysis of Its States, Phys. Rev. Lett. 89 (2002) 213401.
[10] W. Bertsche, A. Boston, P.D. Bowe, C.L. Cesar, S. Chapman, M. Charlton, M. Chartier, A. Deutsch, J. Dilling, J. Fajans, et al., ALPHA collaboration, The ALPHA Experiment: A Cold Anti-Hydrogen Trap, Prepared for International Conference on Low Energy Antiproton Physics (LEAP'05), Bonn, Juelich, Germany, 16–22 May 2005. Published in AIP Conference Proceedings 796, pp. 301–308, 2005. Also in Bonn 2005, Low Energy Antiproton Physics, pp. 301–308.
[11] W. Bertsche, A. Boston, P.D. Bowe, C.L. Cesar, S. Chapman, M. Charlton, M. Chartier, A. Deutsch, J. Dilling, J. Fajans, ALPHA collaboration, A Magnetic trap for antihydrogen confinement, Nuclear Instruments and Methods in Physics Research A 566 (2006) 746–756.
[12] J. Fajans, W. Bertsche, K. Burke, S.F. Chapman, D.P. van der Werf, Effects of extreme magnetic quadrupole fields on penning traps and the consequences for antihydrogen trapping, Phys. Rev. Lett. 95 (2005) 155001.
[13] J. Fajans, A. Schmidt, Malmberg-Penning and Minimum-B Trap compatibility: the advantages of higher-order multipole traps, Nucl. Instrum. Meth. Phys. Res. A 521 (2004) 318.

[14] K. Gomberoff et al., Simulations of plasma confinement in an antihydrogen trap, Phys. Plasmas (2006) (to be submitted for publication).
[15] ALPHA experiment, AD-5 and CERN, 2005–2006.
[16] F. Peinetti, F. Peano, G. Coppa, J. Wurtele, Particle-in-cell method for parallel dynamics in magnetized electron plasmas: study of high-amplitude BGK modes, J. Comput. Phys. 218 (2006) 102.
[17] G. Andresen, W. Bertsche, A. Boston, P.D. Bowe, C.L. Cesar, S. Chapman, M. Charlton, M. Chartier, A. Deutsch, J. Fajans, M.C. Fujiwara, R. Funakoshi, D. Gill, K. Gomberoff, J.S. Hangst, R. Hayano, Hydomako, M.J. Jenkins, L.V. Jørgensen, L. Kurchaninov, N. Madsen, Nolan, K. Olchanski, A. Olin, A. Povilus, F. Robicheaux, E. Sarid, D.M. Silveira, J.W. Storey, H.H. Telle, R.I. Thompson, D.P. van der Werf, J. Wurtele, Y. Yamazak, ALPHA collaboration, Antimatter plasmas in a multipole trap for antihydrogen, Phys. Rev. Lett 98 (2007) 023402.
[18] D.P. Grote, Alex Friedman, Irving Haber, Jean-Luc Vay, The WARP code: modeling high intensity ion beams, in: Proceedings of the 2004 ECRIS Workshop, AIP Conference Proceedings, vol. 749, issue 1, March 15, 2005, pp. 55–58.
[19] R.H. Cohen, A. Friedman, M. Kireeff Covo, S.M. Lund, A.W. Molvik, F.M. Bieniosek, P.A. Seidl, J.-L. Vay, P. Stoltz, S. Veitzer, Simulating electron clouds in heavy-ion accelerators, Phys. Plasmas 12 (5) (2005) 56718-1-10.
[20] V. Gorgadze, T. Pasquini, J. Fajans, J.S. Wurtele, Injection into electron plasma traps, in: M. Schauer, T. Mitchell, R. Nebel (Eds.), Non-Neutral Plasma Physics V, AIP 692, American Institute of Physics, New York, 2003, p. 30.
[21] A. Friedman, Simulation studies of the stability of weak and strong ion layers and rings, Ph.D. Thesis, Cornell University, 1980.
[22] A. Friedman, J. Denavit, R.N. Sudan, Strong ion ring equilibria formed by injection and intrinsic stochasticity of orbits, J. Comput. Phys. 44 (1981) 104.
[23] A. Friedman, R.N. Sudan, Jacques Denavit, Stability of field reversed ion rings, Phys. Fluids 29 (1986) 3317.